

Analytical approach to the design of a high-force density double-sided linear switched reluctance motor

J. Garcia Amorós¹, P. Andrada²

¹ Departament d'Enginyeria Electrònica, Elèctrica i Automàtica
E.T.S.E., Universitat Rovira i Virgili
Avinguda Països Catalans, 26, 43007 Tarragona, Spain
Tel.:+34 977 559695, fax:+34 977559605
E-mail: jordi.garcia-amoros@urv.cat

² GAECE. Grup d'Accionaments Elèctrics amb Commutació Electrònica
Departament d'Enginyeria Elèctrica, EPSEVG, Universitat Politècnica de Catalunya UPC
Víctor Balaguer s/n, 08800 Vilanova i la Geltrú, Spain
Tel.:+34 938967732; fax: +34 938967700
E-mail: pere.andrada@upc.edu

Abstract. This paper presents an analytical approach to the design of a high-force density double-sided linear switched reluctance motor (LSRM). The design is based on an analytical formulation of the average propulsion force determined using the non-linear energy conversion loop, in which the unaligned magnetization curve is assumed to be a straight line and the aligned magnetization curve is represented by two straight lines. The main dimensions of the LSRM are determined in accordance with the machine requirements, the proposed average propulsion force formula and the geometrical relationships that were presented in a previous paper. The present paper uses two dimensional finite element analysis that has been corrected to take into account the end effects in order to refine and/or to validate the proposed design. Finally an LSRM prototype was built following the proposed design and was verified by experimental measurements.

Key words

Design, analytical force calculations, linear motors, switched reluctance motors,

1. Introduction

Linear Switched Reluctance Motors (LSRMs) are becoming increasingly attractive candidates for use as linear drives for several reasons: they only have concentrated windings on the stator or translator, they are ruggedly built, they have low expected manufacturing costs, and they have good fault-tolerance capability [1]. LSRMs can be classified as transverse flux or longitudinal flux. With transverse flux LSRMs, the plane that contains the flux lines is perpendicular to the line of movement. Reference [2] presents a design procedure for transverse flux LSRMs. In longitudinal flux LSRMs, the plane that contains the flux lines is parallel to the line of

movement. Reference [3] describes a design procedure for longitudinal flux LSRMs. Other types of longitudinal flux LSRMs are presented in [4], with coupled flux paths, and in [5] with uncoupled flux paths for a magnetic levitation system. Reference [6] analyzes a high-force longitudinal flux double-sided double-translator LSRM. Recently, longitudinal LSRMs have been proposed for applications such as precise motion control ([7], [8]), as propulsion systems for railway vehicles [9] and for vertical elevators ([10], [11] [12]). The purpose of this paper is to give an analytical approach to the design of LSRMs. The study focuses solely on longitudinal flux LSRMs for high force density applications; therefore, transverse LSRMs are outside the scope of this study. The paper is organized as follows: Section 2 proposes a formula for determining the LSRM's average propulsion force on the basis of the energy conversion loop. Section 3 outlines the design procedure and applies it to a specific LSRM. Section 4 presents the two dimensional finite element analysis corrected according to the end effects. Section 5 describes the experimental validation. Section 6 presents the conclusions drawn from this research.

2. Analytical approach

This study was conducted using a high-force density LSRM. This LSRM consists of M series connected modules, each one formed by a poly-phase double-sided magnetic structure with N_p active poles per side and N_s passive poles per side. Fig. 1 shows one module of the LSRM along with the geometrical parameters considered in this research, which are b_p , c_p , l_p , b_s , c_s , l_s , L_W , h_y and g . The number of phases (m) and the stroke (PS) can be used as design parameters to determine T_p , T_s , N_p and N_s by means of the following equations:

$$\left. \begin{aligned} T_p &= \frac{1}{2} N_s \cdot PS = b_p + c_p \\ T_s &= \frac{1}{2} N_p \cdot PS = b_s + c_s \end{aligned} \right\} \quad (1)$$

Where,

$$\left. \begin{aligned} N_p &= 2 \cdot m \\ N_s &= 2 \cdot (m \pm 1) \end{aligned} \right\} \quad (2)$$

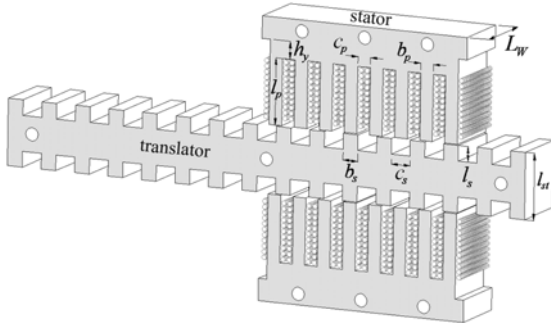


Fig. 1. 3D view of one module ($M=1$) and the main dimensions of the LSRM ($N_p = 8, N_s = 6$)

Average propulsion force can be calculated using an idealized non-linear energy conversion loop in which the unaligned magnetization curve is assumed to be a straight line and the aligned magnetization curve is represented by two straight lines [13].

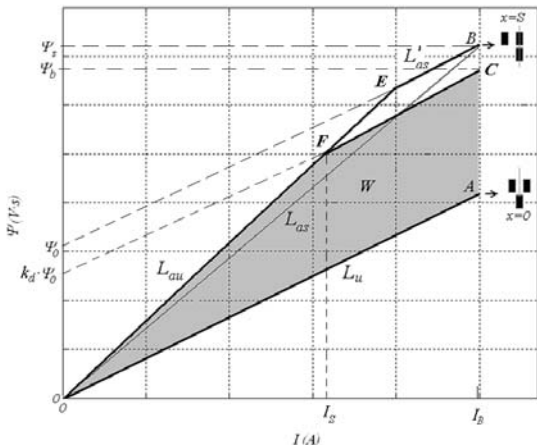


Fig. 2. Idealized non-linear energy conversion loop

This simplified model accounts for the saturation effect and is described in Fig. 2 by means of the lines OA (OA slope= L_u), EB (EB slope= L'_{as}) and OE (OE slope= L_{au}). One of the limitations of the model is that the lines OA and EB are parallel and usually have saturated conditions $L'_{as} < L_u$. Assuming a flat-topped current waveform, the area OACFO is the energy conversion area (W). Excluding iron and friction losses, the average propulsion force per phase ($F_{X,avg}$) is then obtained by:

$$F_{X,avg} = \frac{W}{S \cdot k_d} \quad (3)$$

Where k_d is the magnetic duty cycle factor defined as $k_d = x_c / S$ and S is the distance between the aligned and unaligned positions given by:

$$S = (b_s + c_s) / 2 \quad (4)$$

From Fig. 2 the following expressions can be derived:

$$W = \psi_0 \cdot \left(I_B - \frac{1}{2} I_s \right) \cdot k_d \quad (5)$$

$$\psi_0 = I_B \cdot (L_{as} - L_u) \quad (6)$$

$$I_s \cdot (L_{au} - L_u) = k_d \cdot (L_{as} - L_u) \cdot I_B \quad (7)$$

Inserting (6) and (7) into (5) and operating:

$$W = I_B^2 \cdot L_{as} \cdot K_L \cdot k_d \quad (8)$$

Where K_L is a dimensionless coefficient defined by:

$$K_L = \left(1 - \frac{L_u}{L_{as}} \right) \cdot \left(1 - \frac{1}{2} \cdot \frac{L_{as} - L_u}{L_{au} - L_u} \cdot k_d \right) \quad (9)$$

At point B (see Fig. 2) the poles are fully aligned and therefore:

$$\psi_s = L_{as} \cdot I_B = B_p \cdot N_l \cdot N_{pp} \cdot b_p \cdot L_w \quad (10)$$

Where N_l is the number of coils per pole, N_{pp} the number of stator poles per phase and B_p the magnetic flux density in the stator pole.

The total ampere-turns per slot ($N_l \cdot I_B$) can be expressed, with the slot fill factor (K_s), by means of the current density peak (J_B) by:

$$N_l \cdot I_B = K_s \cdot \frac{c_p \cdot l_p}{2} \cdot J_B \quad (11)$$

Inserting (10) and (11) into (8)

$$W = \frac{1}{2} \cdot (K_L \cdot K_s \cdot k_d) \cdot (c_p \cdot b_p \cdot l_p \cdot L_w \cdot N_{pp}) \cdot (B_p \cdot J_B) \quad (12)$$

The number of stator poles per phase (N_{pp}) in a double-sided LSRM is 4 (see Fig. 1). The double-sided LSRM has the advantage that the translator does not support electromagnetic normal force; therefore the mechanical losses due to friction are minimal, whereas in the single-sided LSRM the normal force between stator and translator can reach more than 10 times the propulsion force.

Inserting (12) in (3) and using (1), the average propulsion force per phase is:

$$F_{X,avg} = M \cdot N_{pp} \cdot \left(\frac{N_s}{N_p} \right) \cdot (K_L \cdot K_s) \cdot \left(\frac{c_p \cdot b_p \cdot l_p \cdot L_w}{T_p} \right) \cdot (B_p \cdot J_B) \quad (13)$$

In order to obtain dimensionless variables, the geometrical variables depicted in Fig. 1 are normalized by the stator pole pitch (T_p), which obtains:

$$\alpha_p = b_p / T_p \quad (14)$$

$$\alpha_s = b_s / T_p \quad (15)$$

$$\beta_p = l_p / T_p \quad (16)$$

$$\beta_s = l_s / T_p \quad (17)$$

$$\gamma_w = L_w / T_p \quad (18)$$

$$\delta_y = h_y / T_p \quad (19)$$

Consequently, (13) can be rewritten as:

$$F_{X,avg} = M \cdot N_{pp} \cdot \left(\frac{N_s}{N_p} \right) \cdot (K_L \cdot K_s) \cdot (\alpha_p - \alpha_p^2) \cdot \beta_p \cdot \gamma_w \cdot T_p^3 \cdot (B_p \cdot J_B) \quad (20)$$

The influence of the geometrical parameters on the force profile of a double-sided LSRM has been investigated in [14, 15]. If the maximum average force has to be an optimizing factor, the following rules concerning the geometrical parameters could be useful:

- 1) Primary pole width should be $\alpha_p = 0.4167$ or $b_p = T_p / 2.4$
- 2) Secondary pole width should be $\alpha_s = 0.5$ or $b_s = T_p / 2$

- 3) The relation $b_s=1.2 b_p$ is a suitable design criterion for the pole widths.
- 4) Translator pole length should be $\beta_s=0.5$ or $l_s=T_p/2$
- 5) Stator pole length should be $\beta_p=2.5$
- 6) Stack length (L_W) is made to match the average force to the values expected from the design because the average force is proportional to L_W . Nevertheless an excessive stack increases the mass and iron losses.
- 7) Yoke length should be $\delta_y=0.5417$ or $h_y=T_p/1.846$ to avoid saturation and loss of average thrust. Higher values do not have any influence and only increase the stator mass.
- 8) The air gap length (g) should be as small as possible to maximize the average force compatible with tolerances and manufacturing facilities.

If the average force per unit of copper mass has to be considered then the best value for the primary pole width is $\alpha_p=0.5$ or $b_p=T_p/2$.

The K_L coefficient depends on the geometrical parameters and the current density. Table I shows the recommended intervals for K_L .

Table I. – Intervals for K_L

$J=5A/mm^2$	$0.268 \leq K_L \leq 0.304$
$J=10A/mm^2$	$0.272 \leq K_L \leq 0.330$
$J=15A/mm^2$	$0.215 \leq K_L \leq 0.292$
$J=20A/mm^2$	$0.158 \leq K_L \leq 0.247$

The magnetic flux density in the stator pole, B_p , is conditioned by the maximum value at which laminations reach magnetic saturation. The current density, J_B , strongly depends on operating conditions and cooling facilities.

3. Design procedure

When designing an LSRM, the parameters and dimensions which define the motor and the power converter are fixed in order to verify certain previously defined requirements (i.e. number of phases, force, speed) and constraints (i.e. voltage, temperature rise and some specific dimensions). Once the requirements and constraints have been established, by means of equation (20) and following the guidelines given in Section 2, the main dimensions of the LSRM are derived.

The maximum flux linkage at point B (see Fig. 2), at a constant speed u_b , with flat-topped current waveform and neglecting resistance, is related to the DC voltage V_b by means of:

$$\psi_0 = \frac{V_b \cdot S}{u_b} \quad (21)$$

Thus:

$$\psi_0 = \psi_s \left(1 - \frac{L_u}{L_{as}} \right) \quad (22)$$

Then from equation (10) the number of turns per pole is given by:

$$N_1 = \frac{V_b \cdot S}{N_{pp} \cdot M \cdot b_p \cdot L_w \cdot u_b \cdot B_p \cdot (1 - L_u / L_{as})} \quad (23)$$

A four phase ($N_p = 8$, $N_s = 6$) double-sided linear switched motor was designed in order to illustrate the proposed procedure. The average force propulsion was 25 N, the speed (u_b) was 17 m/s, voltage (V_b) was 12 V and the power converter was a classic converter. The main dimensions obtained following the aforementioned procedure are shown in Table II.

Table II. – LSRM prototype main dimensions

Number of phases	m	4
Number of modules	M	1
Stator pole width	b_p	6 (mm)
Stator slot width	c_p	6 (mm)
Stator pole pitch	T_p	12 (mm)
Number of active poles per side	N_p	8
Stator pole length	l_p	30 (mm)
Translator pole width	b_s	7 (mm)
Translator slot width	c_s	9 (mm)
Translator pole pitch	T_s	16 (mm)
Number of passive poles per side	N_s	6
Translator pole length	l_s	7 (mm)
Yoke length	h_y	8 (mm)
Stack length	L_W	30 (mm)
Air gap length	g	0.5 (mm)
Stroke	PS	4 (mm)
Number of turns per pole	N_j	11
Wire diameter	d_c	2.1 (mm)
Duty cycle factor	k_d	0.4
Current density	J_B	15 (A/mm ²)
Flux density in stator pole	B_p	1.8 (T)
Lamination steel		FeV 270-50HA

4. Finite element analysis

After the dimensions have been fixed (as described in Section 3), they need to be refined or validated. The best process for this is two dimensional finite element analysis (2D FEA) that has been adjusted in accordance with the end effects. End effects in 2D FEA are taken into account by means of the end-effects coefficient, K_{ee} , which depends on the current density (J) and position (x), given by:

$$\psi_{3D} = K_{ee} \cdot \psi_{2D} \quad (24)$$

$$L_{3D} = K_{ee} \cdot L_{2D} \quad (25)$$

Where ψ_{2D} and L_{2D} are the flux linkage and the inductance obtained in 2D FEA and ψ_{3D} and L_{3D} are the 3D flux linkage and the inductance approaches that account for the end effects and are most similar to the measured values. The correction factor K_{ee} is defined as [16]:

$$K_{ee} = \left(1 + \frac{L_{end} \cdot K_{si}}{L_{2D}} \right) \cdot K_f \quad (26)$$

Where L_{end} is the end-winding inductance, K_{si} is a factor that affects L_{end} due to the steel imaging effect and K_f is the axial fringing factor. K_{si} can usually be omitted ($K_{si} = 1$) since its effect on L_{end} is generally less than 2%. End-winding inductance, L_{end} , can be analytically deduced from end-winding geometry or can be computed by means of an axis-symmetrical 2D finite element model [17].

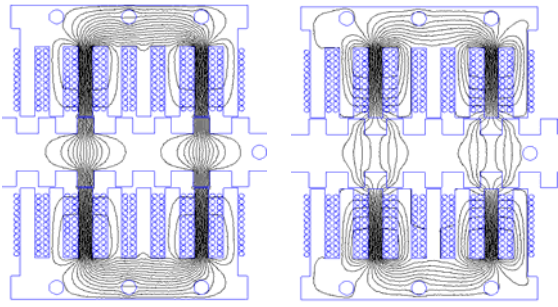


Fig. 3. Flux plots from 2D FEA of the LSRM a) aligned b) unaligned

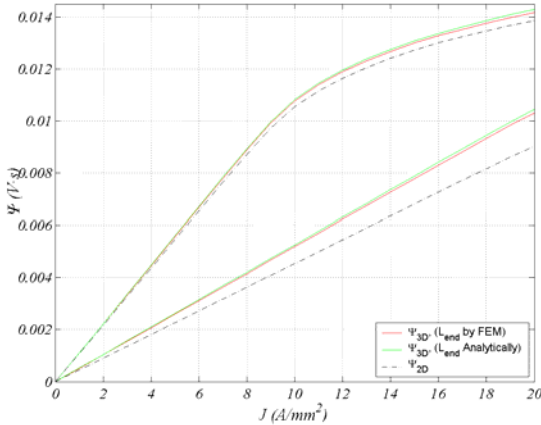


Fig. 4. Corrected Ψ_{3D} for aligned and unaligned positions with L_{end} computed analytically or by FEM

Flux plots obtained by means of 2D FEA in the aligned and unaligned position are shown in Fig. 3. Fig. 4 shows the magnetization curves Ψ_{2D} (flux linkage versus current for the different positions of the translator) obtained by 2D FEA, and the same curves corrected by the end-effect coefficient, Ψ_{3D} . Taking (Ψ_{3D}) into account, the co-energy (W'_{3D}) is calculated using the well-known expression:

$$W'_{3D}(x_i, I) = \int_0^I \psi_{3D}(x, i) \cdot di \Big|_{x_i=Cm} \quad (27)$$

Then, the propulsion force, including the end effects, is obtained by:

$$F_{x,3D}(I) = \frac{\partial W'_{3D}(x, I)}{\partial x} \Big|_{I=Cm} \quad (28)$$

The influence of the end effects on the propulsion force is clearly shown in Fig.5.

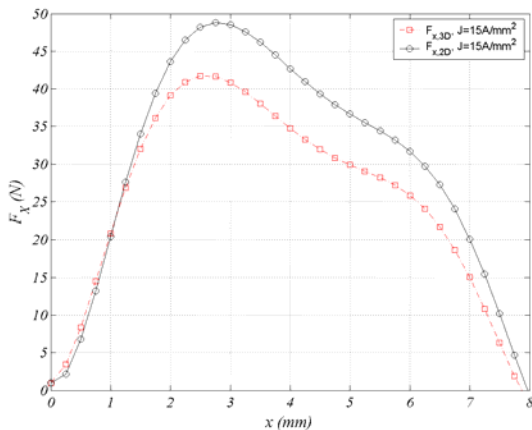


Fig. 5. 2D and 3D propulsion force

5. Experimental results

The LSRM was tested in order to evaluate the proposed design procedure. A test setup was built to perform the experimental measurements (Fig. 6 and Fig. 7). The flux linkage-current curves were obtained following the procedure described in [18]. Fig. 8 compares the results obtained with the proposed procedure, 2D FEA (corrected according to the end effects), and the experimental test of magnetization curves (Ψ_{3D} vs. I) in the aligned and unaligned positions. Fig.9 shows the measured force versus the values derived from equation (28). Finally, the average force propulsion values are listed in Table III.



Fig. 6. View of the test setup and of the double-sided LSRM

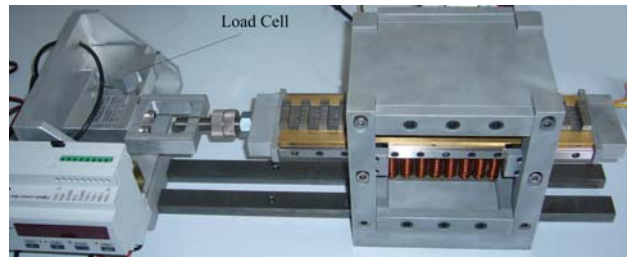


Fig. 7. View of the test setup and load cell detail

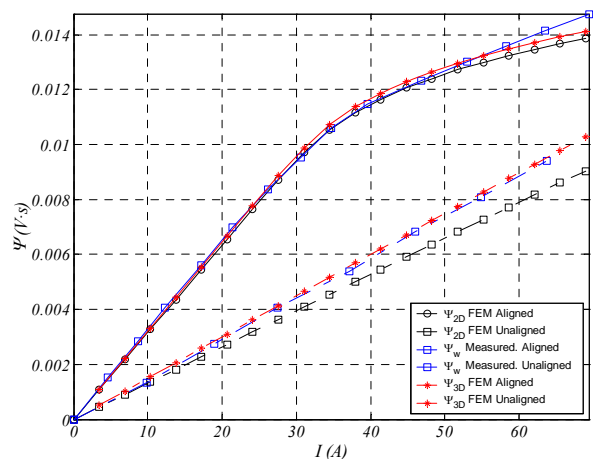


Fig. 8. Ψ_{2D} , Ψ_{3D} and measured flux linkage vs. current for aligned and unaligned position

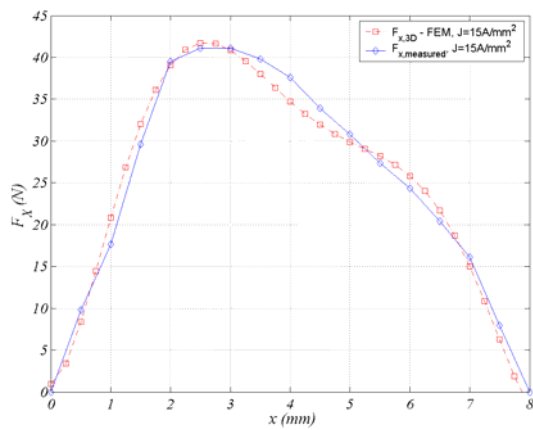


Fig. 9. 3D and measured propulsion force.

Table III. – Average force results ($J=15A/mm^2$)

FEM	$F_{x,avg}$	25.1 (N)
Analytical expression (20)	$F_{x,avg}$	23.2 (N)
Measured values	$F_{x,avg}$	24.5 (N)

6. Conclusion

This paper presents an analytical approach to the design of a high-force density double-sided linear switched reluctance motor (LSRM). The design is based on an analytical formulation of the average propulsion force determined using the non-linear energy conversion loop. Main dimensions of the LSRM are determined according to the machine requirements, the proposed average propulsion force formula and the geometrical relationships that were presented in a previous paper. 2D FEA corrected in order to take into account the end effects is used to refine and/or to validate the proposed design. Finally an LSRM prototype was built according to the proposed design. Experimental tests validated the proposed procedure.

Acknowledgement

The authors would like to thank Talleres Petit, Tarragona, Spain, for assembling the prototype. This research was supported by the Spanish Ministry of Education and Science and the European Regional Development Fund (DPI2006-09880 and DPI2007-66872).

References

[1] Miller T. J. E., *Switched Reluctance Motor and their Control*, Magna Physics Publishing and Clarendon Press Oxford 1993.

[2] Baoming, G.; de Almeida, A.T.; Ferreira, F., "Design of Transverse Flux Linear Switched Reluctance Motor", *IEEE Transactions on Magnetics*, vol.45, no.1, pp.113-119, Jan. 2009

[3] Byeong-Seok L., Han-Kyung B., Praveen V., Krishnan R., "Design of a linear switched reluctance machine", *IEEE Transactions on Industry Applications*, vol. 36, no. 6, pp. 1571-1580, Nov/Dec 2000

[4] Chayopitak, N.; Taylor, D.G., "Design of linear variable reluctance motor using computer-aided design assistant"

IEEE International Conference on Electric Machines and Drives, pp.1569-1575, May 2005

[5] Zhengang Sun; Cheung, N.C.; Jianfei Pan, Shi Wei Zhao, Wai-Chuen Gan, "Design and simulation of a magnetic levitated switched reluctance linear actuator system for high precision application" *IEEE International Symposium on Industrial Electronics, ISIE 2008.*, pp.624-629, June 30 2008-July 2 2008

[6] Deshpande U.S.; Cathey J.J.; Richter, E., "High-force density linear switched reluctance machine", *IEEE Transactions on Industry Applications*, vol.31, no.2, pp.345-352, Mar/Apr 1995

[7] Pan J.; Cheung N.C.; Jinming Yang, "High-precision position control of a novel planar switched reluctance motor", *IEEE Transactions on Industrial Electronics*, , vol.52, no.6, pp. 1644-1652, Dec. 2005

[8] Zhao S. W., Cheung, N.C.; Wai-Chuen Gan; Jin Ming Yang; Jian Fei Pan, "A Self-Tuning Regulator for the High-Precision Position Control of a Linear Switched Reluctance Motor", *IEEE Transactions on Industrial Electronics*, vol.54, no.5, pp.2425-2434, Oct. 2007

[9] Kolomeitsev L., Kraynov D., Pakhomin F., Rednov F., Kallenbach E., Kireev V., Schneider T., Böcker J. "Linear Switched Reluctance Motor as High Efficiency Propulsion System for Railway Vehicles" *Proceedings SPEEDAM 2008*, pp 155-160.

[10] Hong Sun Lim, Krishnan R., "Ropeless Elevator With Linear Switched Reluctance Motor Drive Actuation Systems" *IEEE Transactions on Industrial Electronics*, vol.54, no.4, pp.2209-2218, Aug. 2007

[11] Hong Sun Lim, Krishnan R., Lobo N.S. "Design and control of a Linear Propulsion System for an Elevator Using Linear Switched Reluctance Motor drives". *IEEE Transactions on Industrial Electronics*, vol. 55, no. 2, pp. 534-542. Feb 2008

[12] Lobo N. S, Hong Sun Lim, Krishnan R., "Comparison of Linear Switched Reluctance Machines for Vertical Propulsion Application: Analysis, Design, and Experimental Correlation", *IEEE Transactions on Industry Applications*. vol.44, no. 4, pp. 1134-1142, Aug 2008

[13] Miller T. J. E., "Converter Volt-Ampere Requirements of the Switched Reluctance Motor Drive", *IEEE Transactions on Industry Applications*, vol. IA-21, no. 5, Sep/Oct 1985

[14] Amoros J. G., Andrada P., et al. "Sensitivity Analysis of Several Geometrical Parameters on Linear Switched Reluctance Motor Performance". *Proceedings ICM International Conference on Electrical Machines*, 6-9 Sep 2008, Vilamoura, Portugal.

[15] Amoros, J. G.; Andrada, P., "Sensitivity Analysis of Geometrical Parameters on a Double-Sided Linear Switched Reluctance Motor", *IEEE Transactions on Industrial Electronics*, vol.57, no.1, pp.311-319, January. 2010

[16] Matveev A., Kuzmichev V., Lomonova E., "A new comprehensive approach to estimation of end-effects in switched reluctance motors", *Proceedings ICM International Conference on Electrical Machines*, Bruges, Belgium, August 2002

[17] Amoros J.G., Andrada P. "Study of end effects on the performance of the linear switched reluctance motors" XI CHLIE. 1-4 July 2009, Zaragoza, Spain.

[18] H. Bausch, K. Kanelis, "Feedforward Torque Control of a Switched Reluctance Motor Based on Static Measurement" *European Transactions on Electrical Power*, vol. 7, no. 6, pp. 373-380, November/December 1997.